IOPscience iopscience.iop.org

Home Search Collections Journals About Contact us My IOPscience

A compact model for binary oxides-based memristive interfaces

This content has been downloaded from IOPscience. Please scroll down to see the full text.

2013 J. Phys. D: Appl. Phys. 46 415101

(http://iopscience.iop.org/0022-3727/46/41/415101)

View the table of contents for this issue, or go to the journal homepage for more

Download details:

IP Address: 200.0.233.52
This content was downloaded on 21/10/2013 at 15:44

Please note that terms and conditions apply.

J. Phys. D: Appl. Phys. 46 (2013) 415101 (6pp) doi:10.1088/0022-3727/46/41/415101

A compact model for binary oxides-based memristive interfaces

Néstor Ghenzi[1], **María José Sánchez**[2] **and Pablo Levy**[3]

[1] INN-GIANN, CAC-CNEA, Av. Gral Paz 1499 (1650) San Martín, Argentina
[2] INN-GIANN, Centro Atómico Bariloche and Instituto Balseiro, CNEA, 8400 San Carlos de Bariloche, Río Negro, Argentina
[3] INN-GIANN, CAC-CNEA, Av. Gral Paz 1499 (1650) San Martín, Argentina

Received 11 July 2013, in final form 19 August 2013
Published 23 September 2013
Online at stacks.iop.org/JPhysD/46/415101

Abstract

We report the resistive switching (RS) characteristics of Al/TiO_2/Au memristive cells fabricated in a crossbar array. The measured R–V curves suggest that RS takes place essentially at the Au/TiO_2 interface. We propose a model based on the electric field enhanced migration of oxygen vacancies at that interface which reproduces the main features of the experimental data, namely the remnant resistance states and the degradation process. Obtained vacancy profiles at the active region of the junction give insight for the design of improved devices.

(Some figures may appear in colour only in the online journal)

1. Introduction

A considerable effort is devoted today to develop the next generation of memory devices capable of overcoming the downscaling limitations of actual flash memories. Among the emerging candidates, the resistive random access memories (ReRAM) based on metal/transition metal oxides(TMO)/metal cells attract attention, exhibiting fast read/erase operations with promising characteristics for high-density integration. Its operation relies on the resistive switching (RS) effect, i.e. the reversible change of the resistance between two well-defined values, high (HR) and low (LR) resistance states, after the application of electric pulses. The transition from HR to LR is driven by a SET stimulus, while a RESET pulse settles the transition from the LR to the HR state. In the case of SET/RESET transitions controlled by voltages of different polarities the RS is named bipolar, otherwise it is called unipolar [1, 2]. Bipolar RS exhibits, in general, a better stability than the unipolar mode.

Memory cells based on binary oxides (BO) usually have a high compatibility with CMOS integration and retention times of more than 10^6 s [3, 4]. A large variety of BO has been explored for ReRAM applications, such as NiO [5], ZnO [6], WO [7], HfO_2 [8], CuO [9, 10] and TiO_2 [11] among others. In particular, TiO_2 cells have been the target of many recent studies, since their identification as the first physical example of a solid state memristive device [12], in which fundamental properties of circuit theory and artificial neural networks could be tested.

Despite the fact that several physical mechanisms based in either electron or ion determined RS have been recently suggested in the literature [13–18], all the ingredients involved in this phenomenon have not yet been fully understood.

In this work we focus on the bipolar RS characteristics of Au(50 nm)/TiO_2(100 nm)/Al(50 nm) junctions, fabricated in a crossbar pattern.

A salient feature of our experimental results is the evidence of a single interface—Au/TiO_2—as the active one for the RS. This produces characteristic resistance hysteresis switching loops (HSL), qualitatively different from those obtained in the case of two active interfaces, as will be described below.

The experimental results are qualitatively reproduced by numerical simulations built on a revisited version of the *voltage enhanced oxygen vacancy* (VEOV) model [19]. This model, originally introduced for complex oxides-based memory cells, is adapted here in order to incorporate distinctive and new features of bipolar RS in BO-based memory cells. In addition, the electroforming mechanism and the degradation process are discussed in detail.

2. Device and experiment

We study Al(50 nm)/TiO_2(100 nm)/Au(50 nm) junctions, with areas ranging between 20 μm × 20 μm and 1000 μm × 1000 μm in a crossbar pattern. Amorphous TiO_2 films were deposited by reactive sputtering with a pressure of 20 mTorr, and a power of 150 W at room temperature. The two metals

 © 2013 IOP Publishing Ltd Printed in the UK & the USA

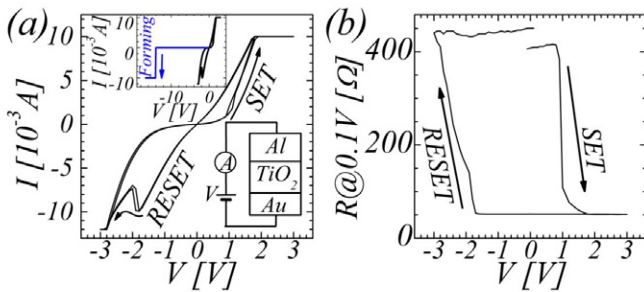

Figure 1. (*a*) Pulsed IV curves measured at room temperature on the Al(50 nm)/TiO_2(100 nm)/Au(50 nm) junction. Inset: electroforming process with a compliance current $I_{cc} = 10$ mA. (*b*) Associated remnant response (HSL) measured after each driving pulse, with a bias voltage of $V = 0.1$ V. The polarity of the voltage is relative to the TE, with the BE grounded. See text for details.

acting as bottom (BE) and top (TE) electrodes were evaporated by the thermal evaporation method. To get the crossbar pattern we employ a lift-off process to define each one of the three layers of the junction (TE = Al, TMO = TiO_2 and BE = Au). The electrical characterization (I–V curves) was performed with a source-measurement unit, Keithley 2400, as it is schematically depicted in the bottom inset of figure 1. In all the measurements, the polarity of the voltage is defined relative to the TE, with the BE grounded.

We shall focus on measurements performed on a specific cell, a 100 μm × 100 μm junction (in the following 'the sample') of the crossbar array, as we observe no dependence of the RS parameters with the area of the junctions.

We measure RS in a two-step process. First, the sample is electroformed at an electric field (applied voltage ≈ -15 V) which abruptly increases the current I (see inset figure 1(*a*)). We set the current compliance I_{cc} at a value of 10 mA. For higher values we have observed unipolar behaviour while for $I_{cc} \lesssim 10$ mA, the bipolar behaviour is obtained (see description below). For the field values used in the electroforming (10^7 V cm^{-1}), close to the dielectric breakdown, it is likely that oxygen species and defects may move (or even be created) by a combined mechanism of drift and diffusion, as a consequence of the applied voltage and the local heating, respectively [20]. After the electroforming process the device is in the OFF state of bipolar RS.

The next step was to analyse the effect of applying electric pulses, including both polarities. The protocol we follow is to apply voltage ramps consisting of pulses (4 ms duration) of increasing amplitude, from 0 to 3 V, then decreasing down to -3 V and finally returning to 0 V to complete one cycle. The current compliance I_{cc} was kept at a level of 10 mA and a time interval of 1 s was taken between pulses to avoid Joule heating.

We observe a typical bipolar RS behaviour, shown in the IV curve of figure 1(*a*), i.e. two branches corresponding to HR and LR states are present. These measurements exhibit the characteristic nonlinear behaviour of the bipolar LR state [21]. Note the current in the RESET process is ~10 mA, a value similar to I_{cc} in the SET process.

In the same run, between pulses we read the remnant two terminal resistance by means of a nondisturbing signal (at a constant voltage of 0.1 V). In figure 1(*b*) we plot the as-obtained resistance HSL. As observed, the remnant resistance exhibits two well-defined resistance values, the LR state around $R_{LR} = 50\,\Omega$ and the HR state at $R_{HR} = 400\,\Omega$ ($R_{HR}/R_{LR} \sim 8$) and two rapid transitions between them. Initially, after the electroforming, the device is in the HR state. At a voltage $V \sim +1$ V it switches to the LR state (SET transition) in which it remains, until, after changing the polarity of the voltage and for $V \sim -2$ V, it switches back again to the HR state (RESET transition). As expected, the SET and RESET transitions observed in the HSL curve are localized at the same voltages as in the IV curve [22].

It is worth mentioning that a squared HSL shape is directly related to the RS effect of a *single interface* [10, 19, 22–25]. On the other hand, when two active interfaces are (deliberately or not) connected in series, the *table with legs* shape [26] evidentiates the overall contribution of each single interface to the RS [19]. Note that this shape resembles the spin valve response (resistance as a function of sweeped magnetic field): the coercive fields of both TE and BE have to be overcomed in order to obtain spin polarized transport [27]. In the RS case, the contribution of each active interface gives additional richness to the available remnant states [19, 26]. This idea has been further developed in the case of complementary devices, i.e. two memory devices connected back to back [28].

Hence, although two metal–oxide interfaces build up our device, the shape of the obtained HSL is illuminating of a *single interface* behaviour. The characteristic polarity response, the work function and electronegativity of the involved metals [29], and the unbalancing role of oxygen vacancies, will be the tools to determine which interface is the active one.

3. The role of oxygen vacancies

Electroforming in these samples was obtained with *negative* voltages. After the forming the device remains in the OFF state of bipolar RS. When *positive* electroforming was tested, we observed no abrupt increase of the current up to 20 V or an unstable RS behaviour.

Therefore we focus on the *negative* polarity electroforming, which renders stable RS properties. In this case, we speculate that oxygen vacancies (positive charge ions) are attracted towards the negative TE, leaving behind oxygen ions, close to the BE.

Generically, oxygen vacancies (OV) in BO act as n-type dopants, transforming the insulating oxide in a conductive doped semiconductor. The motion of OV during electroforming generates a conductive path that tends to shunt the TE and BE. However, the oxygen ions that remain in the neighbourhood of the BE (and even penetrate into it), define a narrow layer that prevents the complete formation of the conductive filament [30].

In addition, an oxygen deficient narrow layer could also be formed naturally near the TE by diffused Al^{3+}, as it has been already reported for some Al/TiO_2 interfaces [31].

Following the preceding description, figure 2 sketches the motion of OV towards the TE (oxygen ions towards the BE), during the transient (negative) electroforming (panels (*a*)–(*b*)).

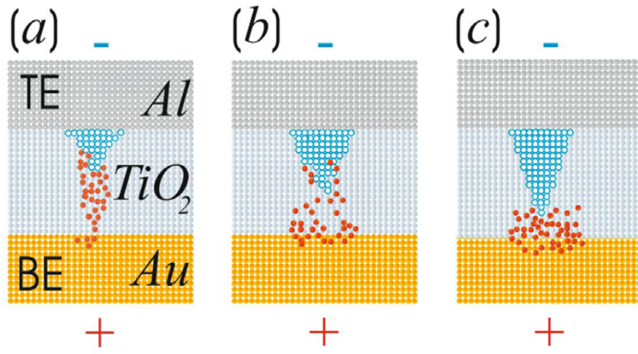

Figure 2. Schematics showing the motion of oxygen species (red filled circles) and oxygen vacancies (blue empty circles) during the negative electroforming transient (panels (*a*)–(*b*)) and final distribution after the sample is formed with the conductive filament (panel (*c*)). Some penetration of oxygen ions into the BE (Au) is assumed.

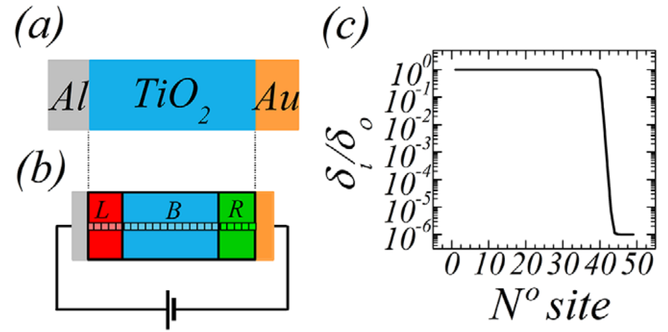

Figure 3. (*a*) Schematics of the experimental sample showing the TE (Al), the 100 nm TiO_2 layer and the BE (Au). (*b*) the device is plotted horizontally to compare to the sample model employed in the simulations, where 50 sites are assigned to the box simulations: the first 10 sites are assigned to the Al/TiO_2 interface (L) while the rightmost 10 sites correspond to the Au/TiO_2 interface (R). The rest of the sites represent the central TiO_2 bulk (B). (*c*) initial density vacancy profile to simulate the OV filament generated in the electroforming.

The final path once the sample is electroformed is displayed at panel (*c*). The cone-shaped filament mimics a local suboxide phase that contains OV in higher densities closer to the TE interface. In this way, the TE (Al/TiO_{2-x}) interface becomes essentially ohmic with a low contact resistance, while the BE—TiO_2/Au(50 nm)—interface is the rectifying non-ohmic one, due to abundance of oxygen ions [2, 20]. The preceding conclusion is in agreement with a recent systematic study of different metal electrodes grown on TiO_2, which classifies and categorizes the I–V response curve of each metal species in terms of the metal work function and electronegativity [29]. Consequently, in our case the BE interface results as the active one in the RS effect, with no participation of the TE interface.

It is nowadays widely accepted that the microscopic origin of the bipolar RS is attributed to the migration of OV along nanometre regions close to the electrodes, during the application of external voltage of different polarities. Direct observation of the migration of OV during the SET/RESET transitions has been reported in several BO thin films [32, 33].

Thus, when a pulse is applied to our device, the local electric field at the BE interface is stronger than the one at the TE interface, due to the much larger value of the local resistivity of the former interface. As the polarity of the electric field defines the direction of ions migration, a strong enough positive pulse will push the OV towards the BE, increasing the OV content there (i.e. reducing the width of the oxygen layer) and thus decreasing the local resistance. This originates the SET transition to the LR state, during which the current compliance I_{cc} prevents the complete formation of the conductive filament. In a similar way to soft and hard breakdown [34], the key parameter to select unipolar or bipolar RS mode is the power dissipation, which determines the severity of oxide breakdown. In this way, the control of I_{cc}, and with it the power dissipation, is crucial to operate the RS in the bipolar mode [35, 36].

Once in the LR state, and after reversing the polarity, a strong enough negative pulse will move back the OV located close to the BE interface towards the bulk region, shortening/breaking the former conductive path and inducing the RESET transition to the HR state. However, the OV profile might be slightly different from the initial one obtained after the electroforming. This process, upon repeating sequences, could eventually generate a drift in the resistance value as a function of the number of voltage cycles, producing a degradation effect.

There are several strategies to bypass the degradation problem. Recently, a pulsing protocol that overcomes this performance limitation in manganite based devices has been proposed [24, 25]. The idea was to tailor the pulsing amplitudes, based on the knowledge of the OV profiles and its dynamics, both disentangled by the VEOV model [19, 25].

4. The VEOV model revisited

Taking into account the previous description we elaborate on the VEOV migration model, previously proposed to explain bipolar RS in complex oxides and manganites [19, 22, 24, 25].

Below we shall introduce the specific ingredients and modifications that we have incorporated in order to adapt the VEOV model to Bipolar RS in BO-based samples.

We consider the active region for conduction as a one-dimensional chain of N links as it is schematically shown in figure 3(*b*). The chain simulates the filament created after the forming process that we described and depicted in figure 2. The links may be physically associated to small domains of nanoscopic dimensions in the suboxide phase (with different OV concentration) of the post-formed sample.

Although the one-dimensional chain might be considered as a crude simplification of the actual 3D geometry, it is in accordance with the experimental evidence indicating that the conduction in the low resistance state is highly inhomogeneous, and takes place along a directional path. In the VEOV model, we only consider the redistribution of oxygen vacancies along nanometric regions due to the effect of an external electric field. This redistribution affects the local resistivity, but we assume that charge neutrality is preserved in the sample.

For the present simulations we take $N = 50$ and assign the first ten sites to the left L (Al/TiO_2) interface, sites 11–40

to the TiO_2 bulk (B) region and the last ten sites to the right R (Au/TiO_2) interface.

As the resistivity of TMO is dramatically affected by the precise oxygen stoichiometry, we characterize each link along the chain by a resistivity ρ_i, which is a function of the *local* OV density content δ_i, at site i along the chain.

As we already mentioned, TiO_2 is an insulator in its virgin state. OVs act as n-type dopants, giving free electrons to the conduction band and thus decreasing its resistivity. Following this line of reasoning, we adopt the most simple relation between conductivity (σ_i) and OV density (δ_i); $\sigma_i = \sigma_\alpha^0 + B_\alpha \delta_i$, where σ_α^0 is the residual conductivity for negligible OV concentration and B_α is a proportional factor that is specific for each region α = L, B and R. Now, if $\rho_i = 1/\sigma_i$ we can write the local resistivity as

$$\rho_i = \frac{\rho_\alpha^0}{1 + A_\alpha \delta_i}, \quad (1)$$

that decreases with the OV content, as required. Defining $\rho_\alpha^0 \equiv 1/\sigma_\alpha^0$, the prefactors $A_i \equiv B_\alpha \rho_\alpha^0$ are independent of δ_i, but are specific for each region L, B and R. We take $A_i = A_L$ for $i = 1, 10$, $A_i = A_B$ for $i = 11, 40$, $A_i = A_R$ for $i = 41, 50$. In addition, since the R interface (TiO_2/Au) is the most resistive one—perhaps owing to the formation of a Schottky barrier type of contact due to the high work function of the Au electrode—we take $A_R > A_L \sim A_B$. In contrast, we assume that the Al/TiO_2 interface forms an ohmic-like contact due to the low work function of the Al electrode. This asymmetry in the electrode materials enhances the resistive response ot the sample due to the *lack of compensation* effect between both electrodes [23], and it is in accordance with our experiments, that suggest that only one interface—the Au/TiO_2—is involved in the RS effect.

Equation (1) is one of the new ingredients of the present version of the VEOV, that we here adapt for BO compounds. It differs from the linear relation $\rho_i \propto \delta_i$ used in the earlier version of the VEOV model for complex oxides (perovskites) memory cells [19].

Following equation (1) we compute the total resistance along the sample as $R = c\sum_{i=1}^{N} \rho_i$. c denotes an unessential geometrical constant related to the dimensions of the domains (which we set to unity).

Another new assumption relies on the initial distribution of OV. Due to the filament originated in the electroforming process we adopt as the initial OV density profile $\delta_i(0)$, the one shown in figure 3(c). This profile takes into account the fact that the largest amount of OV are located close to the L (Al/TiO_2) interface, as it is sketched in figure 2 panel (3).

Given an external stimulus $V(t)$ (the applied voltage protocol between electrodes), the OV density profile at link i is updated at each simulation step according to the following rate probability for transfer from site i to a nearest neighbour $j = i \pm 1$, i.e. $p_{ij} = \delta_i(1 - \delta_j)\exp(-V_\alpha + \Delta V_i)$, which is proportional to the concentration of vacancies present at site i, and to the available concentration at the neighbour domain j.

In the Arrhenius factor, $\exp(-V_\alpha + \Delta V_i)$, ΔV_i is the local potential drop at site i, $\Delta V_i(t) = V_{i+1}(t) - V_i(t)$ with $V_i(t) = V(t)\rho_i/R$. In addition, V_α is a dimensionless constant related to the activation energy for vacancy diffusion in the absence of the external applied voltage.

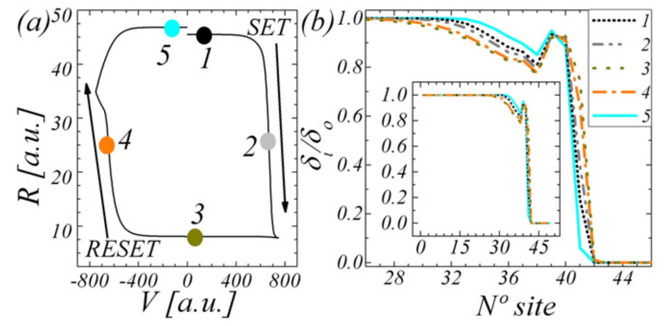

Figure 4. (a) HSL obtained from numerical simulations. See footnote 4 for values of the parameters. (b) Vacancy density profiles in the active R interface in the centre of the electroformed filament, associated with different resistance states marked in (a). Profile labelled 1 corresponds to the HR state at $V = 0$, while 3 corresponds to the LR state at $V = 0$, respectively. In the inset, the vacancy density profiles along the complete 1D chain are shown.

We take $V_\alpha = V0$, for sites in the chain belonging to the L interface and the B region, and $V_\alpha = V1 > V0$ for those sites belonging to the R interface. The different values of V_α stress that, along the conductive filament generated immediately after the electroforming, the rate of diffusion should be larger than along the R interface (see figure 2(c)).

Having in mind the above new ingredients and modifications, the numerical implementation follows straightforwardly: starting from the initial vacancy concentration profile $\delta_i(0)$, at each simulation time step t we compute the local voltage profile $V_i(t)$ and the voltage drops $\Delta V_i(t)$. Employing the probability rates p_{ij} we obtain the transfers between nearest neighbouring sites. Then the values $\delta_i(t)$ are updated to a new set of concentrations $\delta_i(t+1)$, with which we compute, at time $t+1$, the local resistivities $\rho_i(t+1)$ and the local voltage drops under the applied voltage $V(t+1)$, as indicated in the first step.

While in the experiment the current compliance I_{cc} plays a relevant role in order to prevent the damage of the sample in the SET transition, in the simulations the strength of the local electric field at the R interface is essential to determine the net change in the amount of OV density, and thus the change in the total resistance value after the applied pulse $V(t)$.

5. Numerical results

Figure 4(a) shows the HSL obtained from our simulations as a function of applied voltage protocol $V(t)$, starting from the initial density vacancy profile displayed in figure 3(c)[4].

Two stable HR and LR states are displayed, with the same trend for the threshold voltages as in the experimental findings, i.e. coercive thresholds at opposite polarities and steep transitions between states. Besides, the squared type

[4] We normalize the initial OV density profile to $\delta_o = 10^{22}$ OV cm^{-3} which is the typical value reported for the conductive Magneli phase in TiO_2. In this way, $\delta_i(0)/\delta_o \sim 1(\sim 10^{-6})$ on the B side of the conductive filament (R interface). The parameters $V0$ and $V1$ are normalized in units of kT/e. We take $V1 = 12$ ($V0 = 10$), which corresponds to 0.3 eV (0.25 eV) at room temperature. In addition we use $A_L = A_B = 1$ and $A_R = 0.01$, and the ramp voltage is between ±750 (a.u.) with a time constant τ of 5000 time steps.

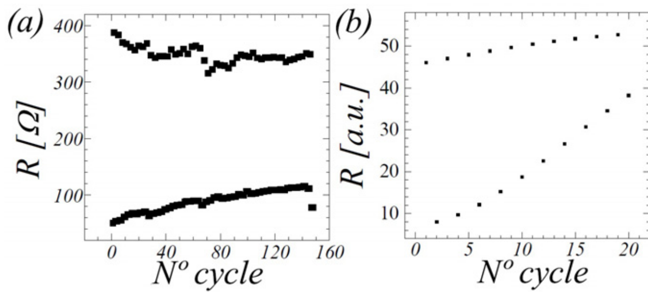

Figure 5. Drift in the HR and LR values as function of the number of voltage cycles: (*a*) experimental and (*b*) numerical results.

HSL is in excellent agreement with the experimental one (figure 1(*b*)), and even exhibits a drift in the resistance value after the completion of a cycle. The drift is originated by a change in the local electric field at the R interface, due to the redistribution of OV (see below).

The *accumulative* drift in the calculated HR and LR values for increasing cycles is in good agreement with the experimental data, obtained from the HR and LR states of HSL cycles measured repeatedly, see figure 5.

The ionic migration does not penetrate deep into the bulk, since there, the much larger conductivity prevents the development of high electric fields. Thus, the main change produced during RS remains confined to the nanometre-size region along the R interface.

Figure 4(*b*) depicts the vacancies density profiles along the 1D chain associated with the LR and HR states at $V = 0$, and for selected intermediate states. A narrow reservoir of oxygen vacancies is formed near the active interface, as shown between sites number 38 and 42. As observed, the profile in the LR state exhibits an accumulation of OV density at the near proximity of the oxide with the metal, resulting in the LR value. On the other hand, the HR state presents less OV content, consistent with model assumptions and equation (1). Note that the OV profiles for both, the transition and the LR states, are smoother than those for the HR state.

The observed experimental degradation after cycling (see figure 5) can be understood when comparing OV profiles 1 and 5 in figure 4(*b*). After a single cycle the OV density at the R interface is slightly smaller than the initial one. This is due to the lower electric field at the bulk B as compared to the R region, which impedes the complete reinjection of OV from the B to the R interface. Then, when cycling, a net drift of oxygen vacancies away from the R interface is produced.

In order to increase the endurance of the devices, a possible route is to perform an asymmetric pulsing protocol, i.e. to adjust the amplitude of each polarity pulse in order to balance the oxygen vacancy drift [24]. Besides, several pulses of the same amplitude could be explored in order to overcome degradation, as is shown in [25].

Recently, a model for RS in Pt/TiO_2/Pt, based on defects diffusion in terms of electrochemical reactions involving oxygen ions/vacancies taking place at a single Pt/TiO_2 interface, has been proposed [23]. The authors elaborated on the presence of the Helmholtz layer, and used a drift diffusion equation and Fick's second law to solve the time-dependent vacancy distribution. We observe a remarkable agreement between their results (i.e. see their figure 4(*b*)) and ours.

This fact strengthens the validity of the VEOV model, originally built on fairly few assumptions [19, 22] and adapted in this work to the case of BO.

6. Conclusions

We observed bipolar RS in TiO_2 based crossbar MIM structures, made using standard microfabrication techniques. After the initial forming we obtained $R_{\mathrm{off}}/R_{\mathrm{on}} \sim 8$, with endurance up to a hundred cycles. By analysing the hysteresis switching loop response, a single active interface has been identified to be responsible for the RS effect.

Our analysis supports two clearly different switching processes in these samples: (1) a soft dielectrical breakdown resulting in the formation of conductive filaments, and (2) diffusion of vacancies enhanced by electrical field. We elaborate on the voltage enhanced oxygen vacancy drift (VEOV) model, originally developed for metal–complex oxide interfaces, to include bipolar switching of a binary oxide based memristive interface. The main new ad-hoc assumptions introduced to tackle this case are relatively simple and general, i.e. the inverse relation between the number of VO and the local resistivity, and the vacancy occupation profiles along the electroformed filament. The lack of area dependence on the RS effect (not reported here) supports our assumption of oxygen vacancies movement along nanoscale conductive channels.

We have shown for this typical memristive TiO_2 based system that our model relying on the electric field enhanced migration of oxygen vacancies at the nanoscale region of the interface reproduces the main features of the experimental curves. The conjunction of simulations data with RS measurements are the key aspect in engineering interfaces for downscaling of ReRAM devices. Moreover, the simulated OV profiles offers the possibility of probing alternative electroforming processes to enhance the RS properties.

Acknowledgments

We acknowledge fruitful discussions with M Rozenberg, P Stoliar and D Rubi. We obtained support from PIP 20080047 'MeMo', MeMOSat Project and PIP11220080101821. NG acknowledges CINN-PRH74 (Argentina). MJS and PL are members of CIC-CONICET.

References

[1] Meijer G I 2008 *Science* **319** 1625
[2] Sawa A 2008 *Mater. Today* **11** 28
[3] Waser R, Dittmann R, Staikov G and Szot K 2009 *Adv. Mater.* **21** 2632
[4] Joshua Yang J *et al* 2012 *MRS Bull.* **37** 131
[5] Ielmini D, Spiga S, Nardi F, Cagli C, Lamperti A, Cianci E and Fanciulli M 2011 *J. Appl. Phys.* **109** 3
[6] Liu Z, Gan J and Yew T 2012 *Appl. Phys. Lett.* **100** 153503
[7] Kugeler C, Rosezin R, Weng R, Waser R, Menzel S, Klopstra B and Bottger U 2009 *9th IEEE Conf. on Nanotechnology (Genova, Italy)* pp 1102–5

[8] Palumbo F, Miranda E, Ghibaudo G and Jousseaume V 2012 *IEEE Electron Device Lett.* **33** 1057
[9] Fujiwara K, Nemoto T, Rozenberg M J, Nakamura Y and Takagi H 2008 *Japan. J. Appl. Phys.* **47** 6266
[10] Ebrahim R, Wu N and Ignatiev A 2012 *J. Appl. Phys.* **112** 123905
[11] Kim H and Kim D W 2011 *Appl. Phys.* A **102** 949
[12] Joshua Yang J *et al* 2008 *Nature Nanotechnol.* **3** 429
[13] Yu S and Wong H 2010 *IEEE Int. Memory Workshop (IMW) (Seoul)* p 54–7
[14] Hur J H *et al* 2010 *Phys. Rev.* B **82** 155321
[15] Makarov A, Sverdlov V and Selberherr S 2011 *J. Vac. Sci. Technol.* B **29** 1
[16] Kim S *et al* 2010 *Appl. Phys. Lett.* **97** 033508
[17] Lin Y S *et al* 2013 *J. Appl. Phys.* **113** 064510
[18] Larentis S 2012 *IEEE Trans. Electron Devices* **59** 2468
[19] Rozenberg M *et al* 2010 *Phys. Rev.* B **81** 115101
[20] Joshua Yang J *et al* 2012 *Nature Nanotechnol.* **8** 13
[21] Joshua Yang J, Strukov D B and Stewart D R 2013 *Nature Nanotechnol.* **8** 13
[22] Ghenzi N *et al* 2010 *J. Appl. Phys.* **107** 093719
[23] Jeong D S, Schroeder H and Waser R 2009 *Phys. Rev.* B **79** 195317
[24] Gomez-Marlasca F *et al* 2011 *Appl. Phys. Lett.* **98** 123502
[25] Ghenzi N *et al* 2012 *J. Appl. Phys.* **111** 084512
[26] Chen X *et al* 2005 *Appl. Phys. Lett.* **87** 233506
Ignatiev R A *et al* 2008 *Phase Transitions* **81** 791
[27] Gregg J F, Petej I, Jouguelet E and Dennis C 2002 *J. Phys. D: Appl. Phys.* **35** R121-55
[28] Linn E *et al* 2010 *Nature Mater.* **9** 403
[29] Zhong N, Shima H and Akinaga H 2010 *Appl. Phys. Lett.* **96** 42107
[30] Pickett M *et al* 2009 *J. Appl. Phys.* **106** 074508
[31] Kim S and Choi Y K 2009 *IEEE Trans. Electron Devices* **56** 3049
[32] Kwon D-H *et al* 2010 *Nature Nanotechnol.* **5** 148
[33] Schroeder H, Pandian R and Miao J 2011 *Phys. Status Solidi* a **208** 300
[34] Jackson J C *et al* 1998 *J. Electrochem. Soc.* **145** 1033
[35] Ghenzi N *et al* 2012 *Physica* B **407** 3096
[36] Jeong D S, Schroeder H and Waser R 2007 *Electrochem. Solid-State Lett.* **10** G51–3